nature portfolio

https://doi.org/10.1038/s41586-022-05087-0

Supplementary information

Anomalous slip in body-centred cubic metals

In the format provided by the authors and unedited

Supplementary Discussion to

Anomalous slip in body-centred cubic metals

Daniel Caillard[1*], Baptiste Bienvenu[2] & Emmanuel Clouet[2*]

[1] *CEMES-CNRS, 29 rue Jeanne Marvig, BP 94347, 31055 Toulouse, France*
[2] *Université Paris-Saclay, CEA, Service de Recherches de Métallurgie Physique, Gif-sur-Yvette 91191, France*
[*] *Corresponding authors.*

We present in this supplementary discussion the elastic energy model used to study the relaxation of the four-dislocation node and the stability of the $\langle 100 \rangle$ junction in BCC metals, as well as additional atomic simulations performed in Nb, W, and Mo to study the mobility of coplanar dislocation networks and the dynamic formation of $\langle 100 \rangle$ junctions.

Outlines:

1) Elastic energy and line energy model
2) Relaxation of a four-dislocation node
3) Formation of a $\langle 100 \rangle$ screw junction reaction
4) Dynamic formation of $\langle 100 \rangle$ junctions in molybdenum
5) Mobility of coplanar dislocation networks
    a. Results in tungsten
    b. Results in niobium
    c. Discussion

1) Elastic energy and line energy model

The elastic energy of a straight infinite dislocation line of character θ is given by [62]:

$$E(\theta) = \frac{b_i[K_{ij}(\theta)]b_j}{4\pi} \ln\left(\frac{R_\infty}{r_C}\right) = e(\theta) \ln\left(\frac{R_\infty}{r_C}\right) \quad (1)$$

where $\vec{b}$ is the Burgers vector of the dislocation, R_∞ is the outer cutoff radius for elastic interactions, r_C is the core radius, and $\overline{\overline{K}}$ is the Stroh tensor, which depends on the elastic constants, on the orientation of the dislocation and on its character θ, i.e. the angle between its Burgers vector and its line direction. An analytical expression of the Stroh tensor $\overline{\overline{K}}$ in the frame of anisotropic elasticity theory is not available for all characters of the dislocation. This tensor is hence calculated numerically, leading to the energy prefactors $e(\theta)$ shown in supplementary Fig. 1 for $1/2\langle 111\rangle$ and $\langle 100\rangle$ dislocations in the different BCC transition metals. The elastic constants and lattice parameters used in this study (Supplementary Tab. 1) are taken from various experimental references and were measured at a temperature of 4.2 K.

Element	a_0	C_{11}	C_{12}	C_{44}	A	m_B
V [63]	3.03	230	120	43	0.78	10.90
Nb [63,64]	3.29	246	132	28	0.50	17.95
Ta [63]	3.30	262	156	83	1.56	6.94
Cr [65]	2.88	392	91	103	0.68	5.55
Mo [66]	3.14	458	168	111	0.77	7.16
W [66]	3.16	517	203	157	1.00	5.88
Fe [67]	2.87	233	135	116	2.38	4.34

Supplementary Table 1: Experimental data used to model dislocations in all BCC transition metals
Bulk lattice parameter a_0 (Å), elastic constants C_{ij} (GPa), resulting elastic anisotropy ratio $A = 2C_{44}/(C_{11} - C_{12})$, and modified bulk to shear moduli ratio $m_B = (C_{11} + 2C_{12})/C_{44}$. Values are taken from various experimental references [63-67].

The elastic energy of a dislocation system is then evaluated with a line-energy approximation thus considering only the elastic self energy of each dislocation segment and neglecting elastic interaction between different segments. This leads to the following elastic energy

$$E^{elas}(\{X_i\}) = \left[\sum_i e(\theta_{i,i+1}) \times L_{i,i+1}\right] \ln\left(\frac{R_\infty}{r_C}\right) \quad (2)$$

where $\theta_{i,i+1}$ and $L_{i,i+1}$ are the character and the length of the dislocation segment joining the two nodes i and $i+1$ located at positions X_i and X_{i+1} respectively.

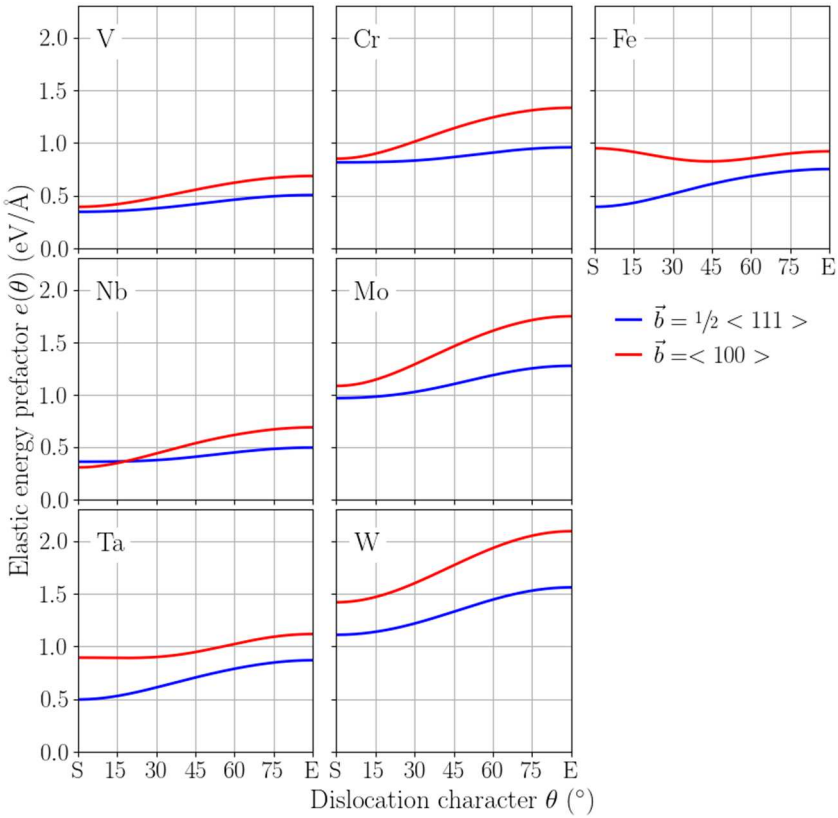

Supplementary Figure 1: Anisotropic elastic energy of straight infinite dislocations.
Elastic energy prefactor $e(\theta)$ of straight infinite dislocations of Burgers vectors $1/2\langle 111\rangle$ (blue) and $\langle 100\rangle$ (red) as a function of their character θ using the anisotropic elastic constants presented in Supplementary Tab. 1.

2) Relaxation of a four-dislocation node

We now use this line energy model to study the relaxation of a quadri-junction formed by four $1/2\langle 111\rangle$ screw dislocation segments intersecting at a node N where the condition $\vec{b}_1 + \vec{b}_2 + \vec{b}_3 + \vec{b}_4 = \vec{0}$ is satisfied. The system is composed of the four dislocation segments, which intersect at the node N and are linked to fixed points at their other ends (Supplementary Fig. 2a). The dislocations, in their screw orientation, have an initial length L_0. Relaxation of the junction leads to glide of the node along the direction $[010]$ defined by the intersection of the slip planes of the four dislocations. After such a glide motion, each dislocation segment acquires the same character θ and has a length $L_0 \cos(\psi_0) / \cos(\psi_0 - \theta)$, where ψ_0 is the angle between the initial screw orientation of the segments and the (010) plane normal to the glide direction of the node. The total elastic energy of the quadri-junction is then given by:

$$E_{QJ}^{elas}(\theta) = 4e(\theta) \times L_0 \frac{\cos(\psi_0)}{\cos(\psi_0 - \theta)} \ln\left(\frac{R_\infty}{r_C}\right). \quad (3)$$

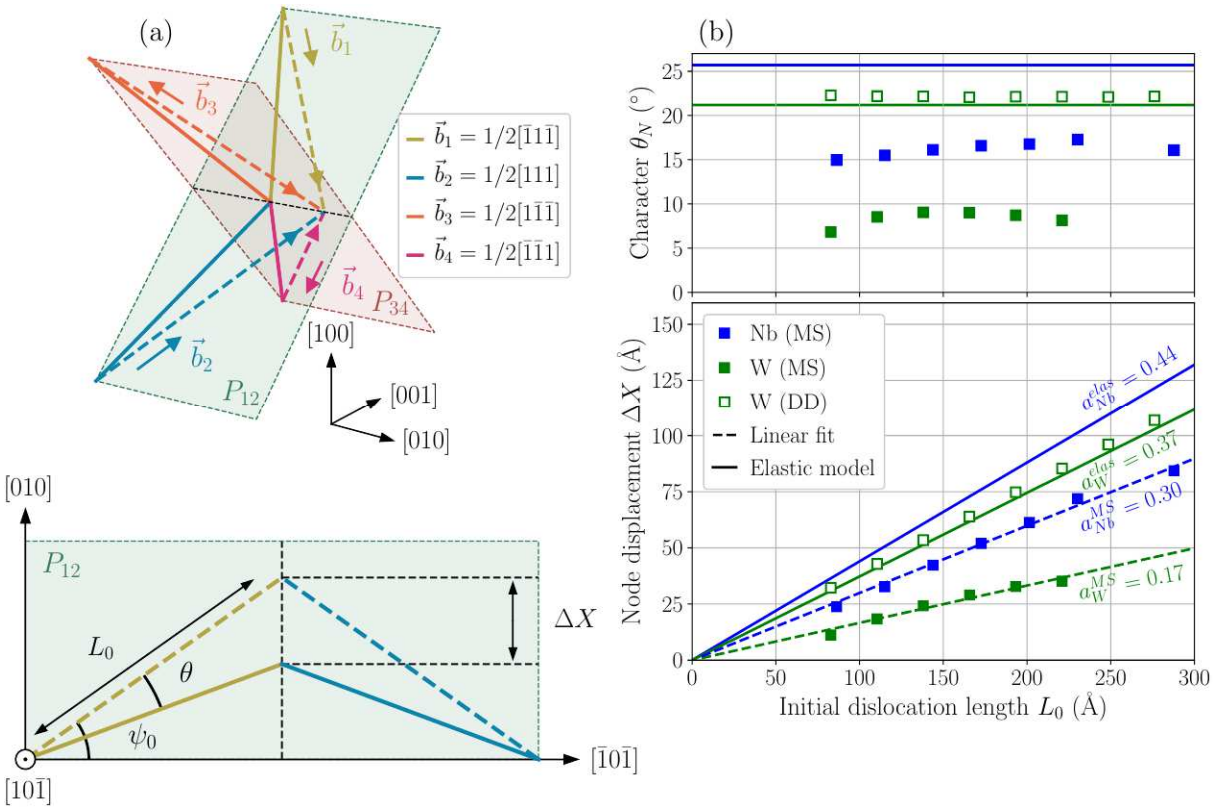

Supplementary Figure 2: Relaxation of the four-dislocation node from elastic and atomistic models. (a) Definition of the notations introduced for formulation of the line energy model of the four-dislocation node with projection onto the P_{12} plane. (b) Equilibrium character θ_N of the four segments (upper panel) and displacement of the node ΔX along the $[010]$ axis (lower panel) as a function of the initial length L_0 of the screw segments. Predictions of the line energy model (solid lines) are compared to results of molecular statics relaxations in Nb and W (filled squares and dashed lines) and of DD simulations in W (open squares).

By minimizing the above equation (3) with respect to the character θ, and replacing the cosines of the angle ψ_0 with its numerical values, we obtain the following equilibrium condition on the character θ_N minimizing the elastic energy of the quadri-junction:

$$\frac{e'(\theta_N)}{e(\theta)} = \tan(\psi_0 - \theta) = \frac{1 - \sqrt{2}\tan(\theta_N)}{\sqrt{2} + \tan(\theta_N)} \tag{4}$$

which has to be solved numerically. The displacement of the node ΔX is then determined geometrically from the value of the equilibrium character θ_N, solution of Eq. (4), and is given by:

$$\frac{\Delta X}{L_0} = \sin(\psi_0) - \cos(\psi_0)\tan(\psi_0 - \theta_N) = \frac{\sqrt{3}}{3}\left[1 - \sqrt{2}\frac{e'(\theta_N)}{e(\theta_N)}\right], \tag{5}$$

showing that the node displacement is proportionnal to the initial length of the dislocation segments.

The results of the line energy model for all BCC transition metals are presented in Supplementary Tab. 2, considering anisotropic elasticity theory with the parameters given in Supplementary Tab. 1. In all BCC metals, relaxation of the quadri-junction forces the four dislocations to leave their screw orientation with an equilibrium character θ_N varying between 10° and 30°, depending on the elastic anisotropy of the BCC metal. The line tension exerted by the four dislocations on the node thus prevents the dislocations from keeping their screw orientation, as observed in our atomistic simulations in niobium, thus allowing for easy glide of these four dislocations connected to the node.

Element	θ_N	$\Delta X/L_0$
V	21.1°	0.37
Nb	25.7°	0.44
Ta	13.0°	0.24
Cr	29.3°	0.49
Mo	24.8°	0.45
W	21.2°	0.37
Fe	10.0°	0.19

Supplementary Table 2: Relaxation of the four-dislocation node according to the line energy model. Equilibrium character θ_N of dislocation segments and displacement ΔX of the node, normalized by the initial length of the dislocation segments L_0, after relaxation of the four-dislocation node.

To validate this line energy model, we compare the model predictions with results of molecular statics relaxation in both Nb and W. A qualitative agreement is found for both metals (Supplementary Fig. 2b). As predicted by the model, the displacement ΔX of the node is proportionnal to the initial length L_0 of the dislocation segments:

$$\Delta X(L_0) = a\, L_0$$

The line energy model predicts a lower slope a in W than in Nb, in agreement with the results of atomistic simulations. In both metals, the slope a observed in atomistic simulations is lower than the one predicted by the model. This difference may be the consequences of atomic effects in the dislocation core or of the elastic interactions between the different dislocation segments which are both neglected in the model.

To better understand this difference between predictions of the line energy model and results of atomistic simulations, we perform additional simulations in tungsten. As the elastic response of tungsten is close to isotropy, one can use isotropic dislocation dynamics (DD) simulations [68] to relax the four-dislocation node. These simulations only consider elasticity and neglect any core contributions, but, contrary to our simple line energy model, they take full account of elastic interactions between the different dislocation segments. These simulations are performed with the DDLab code [69], using a Poisson's ratio $\nu = 0.27$ for W. Relaxation of a four-dislocation node with the isotropic DD code leads to $\Delta X/L_0 = 0.38$ (Supplementary Fig. 2b), in very good agreement with the value $\Delta X/L_0 = 0.37$ given by our line energy model. One can thus conclude that elastic interactions between segments have a negligible impact on the relaxation of the four-dislocation node, with dislocation line energies being the main driving force of this relaxation. The neglect of these elastic interactions in our line energy model is not the reason for the highest slope $\Delta X/L_0$ predicted by the model compared to atomistic simulations. The only contribution left to explain this difference is then the dislocation core energy.

In BCC metals, the screw orientation of the $1/2\,\langle 111\rangle$ dislocation gliding in a $\{110\}$ plane is a minimum of the core energy and corresponds to a marked cusp [70]. Hence, as the four intersecting segments change their characters to trigger the displacement of the node, the core energy, per unit of length, of the four dislocation segments increases. The force resulting from this core contribution tends to maintain the $1/2\,\langle 111\rangle$ dislocation in their screw orientations, partly counterbalancing elastic effects. The neglect of this core contribution in our line energy model could thus be the reason why the model overestimates the slope $\Delta X/L_0$ when compared to atomistic simulations.

Despite this difference on the slope $\Delta X/L_0$ with results of atomistic simulations, the line energy model allows rationalizing the driving forces for the relaxation of the four-dislocation node, showing that the minimization of the dislocation line energy is the main contribution preventing the dislocations to keep their screw orientations when they intersect at such a node. This displacement of the node proportional to the initial length of the four screw dislocation segments corresponds to the situation where no stress is applied to the dislocations. With an applied stress leading to a driving force on the dislocations, as the dislocations are not aligned anymore along their screw orientations, they will easily glide, thus leading to the long distance glide of the four-dislocation node.

3) Formation of a ⟨100⟩ screw junction reaction

In this section, we consider the formation of a ⟨100⟩ screw junction reaction (JR) from two intersecting $1/2\langle 111\rangle$ dislocations of screw character, which are fixed at both ends. For the junction formation to be energetically favourable, the elastic energy needs to decrease upon its formation. The energy variation associated with the junction formation is:

$$\Delta E^{elas}(l_{JR}) = 4\, L_R\, E^{\langle 111\rangle}(\theta) + l_{JR}\, E_S^{\langle 100\rangle} - 4\, L_0\, E_S^{\langle 111\rangle} \qquad (6)$$

with L_0 and L_R the initial and relaxed lengths of the $1/2\langle 111\rangle$ dislocation segments intersecting at the node, and l_{JR} the junction length (see sketch in Supplementary Fig. 3a for notations). The $1/2\langle 111\rangle$ dislocations are initially in screw orientation and have a character θ after formation of the junction, with the corresponding linear energy $E_S^{\langle 111\rangle}$ and $E^{\langle 111\rangle}(\theta)$. $E_S^{\langle 100\rangle}$ is the linear energy of the junction reaction which has a screw orientation.

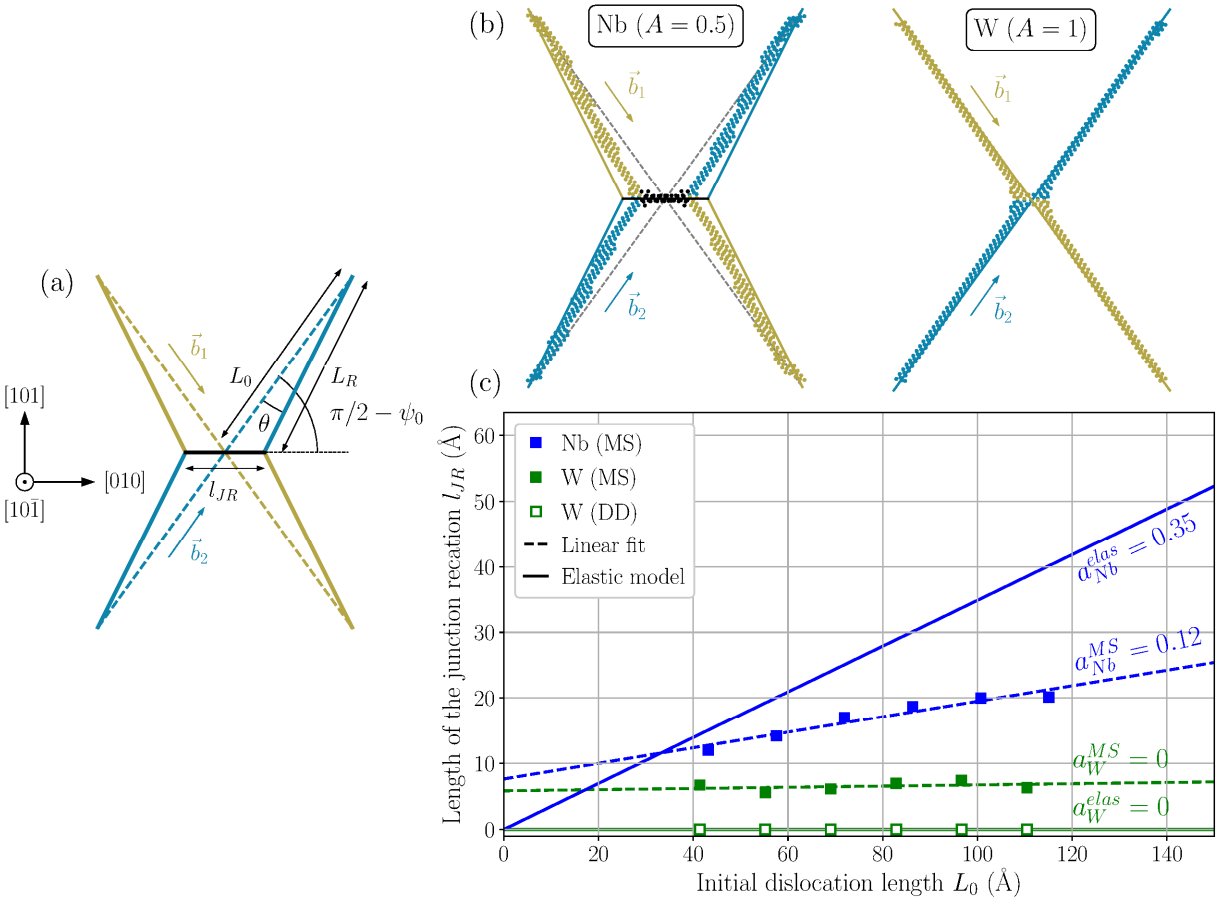

Supplementary Figure 3: Formation of the ⟨100⟩ junction from two intersecting $1/2\langle 111\rangle$ dislocations. (a) Sketch of the formation of a ⟨100⟩ screw junction resulting from the intersection of two initially screw $1/2\langle 111\rangle$ dislocations. (b) Superposition of the relaxed configuration obtained after molecular statics relaxation (coloured spheres) and the predictions of the line energy model (solid lines) for two initially screw $1/2\langle 111\rangle$ dislocations intersecting to form a ⟨100⟩ junction in the case of Nb and W. (c) Length l_{JR} of the junction reaction produced by the intersection of two $1/2\langle 111\rangle$ screw dislocations of length L_0. Predictions of the line energy model (solid lines) are compared to results of molecular statics simulations (filled symbols and dashed lines) for Nb (blue) and W (green), and to results of DD simulations for W (open symbols).

The length of the junction reaction is found by minimizing Eq. (6). To do so, we need first to express the length L_R of the relaxed $1/2\langle 111\rangle$ dislocation segments and their character θ as functions of l_{JR}. Simple geometry leads to the expressions

$$L_R = L_0\sqrt{1 - 2\sin(\psi_0)\frac{l_{JR}}{2L_0} + \left(\frac{l_{JR}}{2\,L_0}\right)^2} = L_0\sqrt{1 - \frac{\sqrt{3}}{3}\frac{l_{JR}}{L_0} + \frac{1}{4}\left(\frac{l_{JR}}{L_0}\right)^2} \tag{7}$$

A good approximate is found by considering a Taylor series expansion of Eq. (7) to the second order in l_{JR}/L_0:

$$\frac{L_R}{L_0} = 1 - \frac{\sqrt{3}}{6}\frac{l_{JR}}{L_0} + \frac{1}{12}\frac{{l_{JR}}^2}{{L_0}^2} + O\left(\frac{{l_{JR}}^3}{{L_0}^3}\right) \tag{8}$$

For the line-energy $E^{\langle 111\rangle}(\theta)$, we use the fact that the $1/2\langle 111\rangle$ dislocations are in screw orientation ($\theta = 0$) in the absence of junction ($l_{JR} = 0$) and that the elastic energy is minimal for the screw dislocation. We thus have

$$E^{\langle 111\rangle}(\theta) = E_S^{\langle 111\rangle} + \frac{1}{2}\frac{\partial^2 E^{\langle 111\rangle}}{\partial\theta^2}\bigg|_{\theta=0}\theta^2 + O(\theta^3) \tag{9}$$

The angle θ is linked to the junction length l_{JR} by the relation

$$\sin(\psi_0 - \theta) = \sin(\psi_0) - \frac{l_{JR}}{2\,L_0} \tag{10}$$

A Taylor series expansion of this relation leads to

$$\theta^2 = \frac{1}{\cos^2(\psi_0)}\left(\frac{l_{JR}}{2\,L_0}\right)^2 + O\left(\frac{{l_{JR}}^3}{{L_0}^3}\right) = \frac{6}{16}\frac{{l_{JR}}^2}{{L_0}^2} + O\left(\frac{{l_{JR}}^3}{{L_0}^3}\right) \tag{11}$$

and then to

$$E^{\langle 111\rangle}(\theta) = E_S^{\langle 111\rangle} + \frac{3}{16}\frac{\partial^2 E^{\langle 111\rangle}}{\partial\theta^2}\bigg|_{\theta=0}\frac{{l_{JR}}^2}{{L_0}^2} + O\left(\frac{{l_{JR}}^3}{{L_0}^3}\right) \tag{12}$$

Injecting these two Taylor series expansions (8) and (12) in the expression (6) of the variation of the elastic energy, we finally obtain

$$\Delta E^{elas}(l_{JR}) = l_{JR}\left\{E_S^{\langle 100\rangle} - 2\frac{\sqrt{3}}{3}E_S^{\langle 111\rangle} + \left[\frac{1}{3}E_S^{\langle 111\rangle} + \frac{3}{2}\frac{\partial^2 E^{\langle 111\rangle}}{\partial\theta^2}\bigg|_{\theta=0}\right]\frac{l_{JR}}{L_0} + O\left(\frac{{l_{JR}}^2}{{L_0}^2}\right)\right\} \tag{13}$$

This function has a minimum for a positive length l_{JR} only if the linear term, $E_S^{\langle 100\rangle} - 2\frac{\sqrt{3}}{3}E_S^{\langle 111\rangle}$, is negative, resulting in the following condition to be satisfied:

$$\alpha_{JR}^{elas} = \frac{\sqrt{3}}{2}\frac{E_S^{\langle 100\rangle}}{E_S^{\langle 111\rangle}} \leq 1 \tag{14}$$

In the frame of isotropic elasticity theory, the ratio between the energies of $1/2\langle 111\rangle$ and $\langle 100\rangle$ screw dislocations is equal to the ratio between the square of the norm of their Burgers vectors, resulting in $\alpha_{JR}^{elas} = 2/\sqrt{3} \approx 1.15$. Hence, according to isotropic elasticity, no $\langle 100\rangle$ junction should form when two $1/2\langle 111\rangle$ screw dislocations intersect. As shown in the main text and in Supplementary Fig. 3b and 3c, this is confirmed by atomistic simulations performed in tungsten, which is almost isotropic. DD simulations [68] performed with DDLab [69] also confirm this result (Supplementary Fig. 3c).

Now considering anisotropic elasticity theory, an analytical expression for the elastic energy of a screw dislocation is available both for $1/2\langle 111\rangle$ and $\langle 100\rangle$ Burgers vectors [71-73]:

$$e_S^{\langle 111\rangle} = \frac{3{a_0}^2 C_{44}}{8\pi}\sqrt{\frac{9+(1+m_B)(2+A)}{(1+2A)[1+A(3+m_B)]}}\ ;\ e_S^{\langle 100\rangle} = \frac{{a_0}^2 C_{44}}{2\pi} \tag{15}$$

where $A = 2C_{44}/(C_{11}-C_{12})$ is the elastic anisotropy ratio and $m_B = (C_{11}+2C_{12})/C_{44}$ is a modified bulk to shear moduli ratio. Their values are given in Supplementary Tab. 1 for all BCC metals. The ratio α_{JR}^{elas} has then an analytical expression given by:

$$\alpha_{JR}^{elas} = \frac{2}{\sqrt{3}} \times \sqrt{\frac{(1+2A)[1+A(3+m_B)]}{9+(1+m_B)(2+A)}} \tag{16}$$

Taking $A = 1$ in the above expression of α_{RJ}^{elas} gives the previous result of isotropic elasticity theory, $\alpha_{JR}^{elas} = 2/\sqrt{3} \approx 1.15$. Considering now elastic anisotropy, one obtains the values in Supplementary Tab. 3 for all BCC metals. The condition for the $\langle 100\rangle$ junction to form is met by all metals satisfying $A \leq 0.8$ (*i.e.* V, Nb, Cr and Mo), almost independently of the value of m_B. Indeed, the elastic energy ratio α_{JR}^{elas} can be approximated as a unique function of the elastic anisotropy A given that $m_B \gg A$:

$$\alpha_{JR}^{elas} \approx \frac{2}{\sqrt{3}} \times \sqrt{\frac{A(1+2A)}{2+A}} \tag{17}$$

The stability condition $\alpha_{JR}^{elas} \leq 1$ is then $8A^2 + A - 6 \leq 0$, which is met for $A \leq \left(-1+\sqrt{193}\right)/16$, i.e. for an elastic anisotropy ratio A smaller than 0.8.

Element	A	$e_S^{\langle 111\rangle}$	$e_S^{\langle 100\rangle}$	α_{JR}^{elas}	l_{JR}/L_0	θ_{JR}
V	0.78	0.35	0.39	0.98	0.01	0.3°
Nb	0.50	0.36	0.31	0.74	0.35	9.0°
Ta	1.56	0.50	0.89	1.56	0	0°
Cr	0.68	0.82	0.85	0.90	0.15	3.6°
Mo	0.77	0.97	1.09	0.97	0.01	0.3°
W	1.00	1.17	1.56	1.11	0	0°
Fe	2.38	0.39	0.95	2.08	0	0°

Supplementary Table 3: Formation of the junction reaction according to the line energy model.
Elastic anisotropy ratio $A = 2C_{44}/(C_{11}-C_{12})$, pre-logarithmic factors $e_S^{\langle 111\rangle}$ and $e_S^{\langle 100\rangle}$ (eV/Å) of the elastic energy of $1/2\langle 111\rangle$ and $\langle 100\rangle$ screw dislocations (eV/Å), elastic ratio α_{JR}^{elas}defining junction stability, normalized equilibrium length l_{JR}/L_0 of the junction reaction and corresponding character θ_{JR} of the two $1/2\langle 111\rangle$ dislocation segments after junction formation.

For metals where the $\langle 100 \rangle$ junction is stable ($\alpha_{JR}^{elas} < 1$), the equilibrium junction length is the minimum of the function $\Delta E^{elas}(l_{JR})$ given by Eq. (13), leading to:

$$\frac{l_{JR}}{L_0} = \frac{2\sqrt{3}E_S^{\langle 111 \rangle} - 3E_S^{\langle 100 \rangle}}{2E_S^{\langle 111 \rangle} + \frac{9}{2}\frac{\partial^2 E^{\langle 111 \rangle}}{\partial \theta^2}\Big|_{\theta=0}} = \frac{\sqrt{3}}{1 + \frac{9}{4E_S^{\langle 111 \rangle}}\frac{\partial^2 E^{\langle 111 \rangle}}{\partial \theta^2}\Big|_{\theta=0}}\left(1 - \alpha_{JR}^{elas}\right) \quad (18)$$

The junction length is thus proportional to the elastic coefficient $\left(1 - \alpha_{JR}^{elas}\right)$. Nb, followed by Cr, have the smallest coefficients α_{JR}^{elas}, indicating that two intersecting $1/2\langle 111 \rangle$ screw dislocations can easily form a $\langle 100 \rangle$ junction in these metals. In V and Mo, this coefficient is close from 1 but still smaller: $\langle 100 \rangle$ junctions are stable but have a small length. Finally, in W, Ta and Fe, this coefficient is larger than 1 and junctions are unstable. This stability of the $\langle 100 \rangle$ directly follows the variations of the elastic anisotropy ratio A, with an increasing stability for small values of A.

To check the validity of the line energy model, we compare its predictions with results of atomistic simulations in Supplementary Fig. 3, where two $1/2\langle 111 \rangle$ screw dislocations intersecting in their middle are relaxed with molecular statics. Atomistic simulations confirm the creation of a junction in niobium, with a length l_{JR} of the junction reaction varying linearly with the length of the two intersecting $1/2\,\langle 111 \rangle$ screw dislocations:

$$l_{JR}(L_0) = a\,L_0 + l_{JR}^0$$

The small offset l_{RJ}^0 appearing in atomistic simulations arises from the uncertainty associated with the measure of the junction length for small junctions. Like for the relaxation of the four-dislocation node, the slope a deduced from atomistic simulations is lower than the one predicted by the line energy model. Here also, one can suppose that the difference arises from the neglect of core contributions in the line energy model. $\langle 100 \rangle$ dislocations have indeed a higher core energy than $1/2\,\langle 111 \rangle$ dislocations. For the screw orientation, empirical interatomic potentials used in this study lead to a core energy equal to 0.48 and 0.25 eV/Å respectively for $\langle 100 \rangle$ and $1/2\,\langle 111 \rangle$ screw dislocations in Nb (0.93 and 0.52 eV/Å in W) for the same core radius $r_c = b_{1/2\langle 111 \rangle} = a_0\sqrt{3}/2$. The highest core energy of the $\langle 100 \rangle$ screw dislocation adds a penalty for the creation of the $\langle 100 \rangle$ junction reaction, which is not considered in the line energy model. It is thus normal that this model overestimate the junction length compared to atomistic simulations. This model, which appears thus semi-quantitative, allows nevertheless to rationalize the impact of elastic anisotropy on the creation of $\langle 100 \rangle$ junction, showing that such junctions are spontaneously created when two $1/2\,\langle 111 \rangle$ screw dislocations intersect in BCC metals where the elastic anisotropy ratio $A = 2C_{44}/(C_{11} - C_{12})$ is smaller than 0.8.

4) Dynamic formation of ⟨100⟩ junctions in molybdenum

Atomistic simulations similar to the ones in tungsten have been performed in molybdenum to study the stability and the elongation of a ⟨100⟩ junction. Results of these simulations are presented in Supplementary Fig. 4.

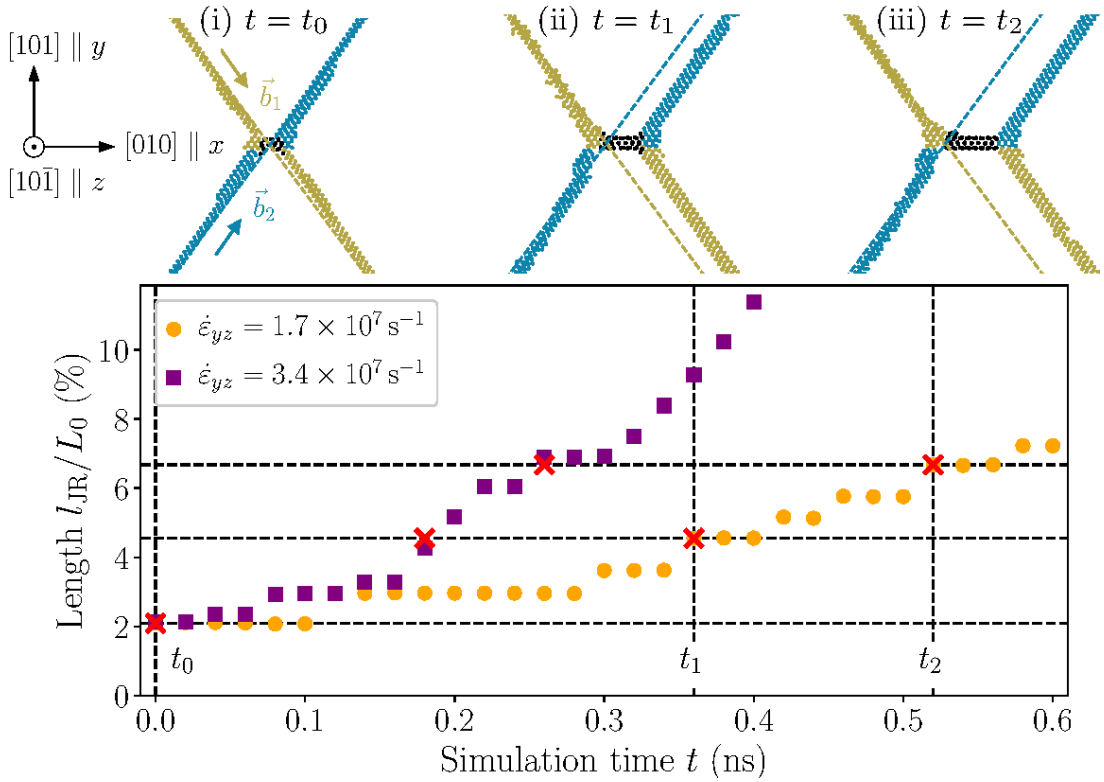

Supplementary Figure 4: Formation of a ⟨100⟩ junction under dynamic conditions in molybdenum. Three snapshots of the MD simulation with $\dot{\varepsilon}_{yz} = 1.7 \times 10^7$ s^{-1} and $T = 100$ K are shown in the upper panel. One can see the elongation of the ⟨100⟩ junction through nucleation of kinks at the right node. The length of the four initial $1/2\,\langle 111\rangle$ screw dislocation arms is $L_0 = 200\,b \simeq 50$ nm. The time evolution of the length l_{JR} of the ⟨100⟩ junction is shown in the lower panel for two different strain rates $\dot{\varepsilon}_{yz}$. The times t_0, t_1 and t_2 of the three MD snapshots are indicated by vertical lines. The initial configuration (i) in t_0 is the result of atomic relaxation by molecular statics at 0 K.

As predicted by the line energy model, a very short ⟨100⟩ junction has spontaneously formed upon the intersection of the two $1/2\,\langle 111\rangle$ screw dislocations, owing to Mo elastic anisotropy ratio $A = 0.77$ being slightly lower than the theoretical threshold ratio 0.8 (see configuration (i) in the upper panel of Supplementary Fig. 4). Under imposed strain rate at $T = 100$ K, the ⟨100⟩ junction starts to expand in its ⟨100⟩ line direction, thanks to the preferred nucleation of kinks at the right node of the junction. This mechanism, observed here in molybdenum, is identical to the one described for tungsten in the main text. MD simulations performed in molybdenum for two different strain rates (lower panel of Supplementary Fig. 4) show a faster junction elongation for an increased strain rate.

5) Mobility of coplanar dislocation networks

We study in this section the motion of a periodic array formed by two intersecting $1/2\,\langle 111\rangle$ screw dislocations, thus forming coplanar dislocation networks, to study their ability to glide cooperatively. Atomic simulations are performed in both W and Nb to see the impact of the elastic anisotropy, and thus of the stability of the $\langle 100\rangle$ junction, on this coplanar motion. In both cases, the simulation cell has a geometry defined by the three vectors $60\,[010]$, $60\,[101]$ and $40\,[10\bar{1}]$, with periodic boundary conditions along the two first directions, X and Y, and free surfaces for the last direction, Z. The screw dislocations with Burgers vectors $\vec{b}_1 = 1/2\,[\bar{1}1\bar{1}]$ and $\vec{b}_2 = 1/2\,[111]$ are introduced in the simulation cell between two opposing corners, as to intersect at the centre of the cell. Their initial length is $120\,b$.

a. Results in tungsten

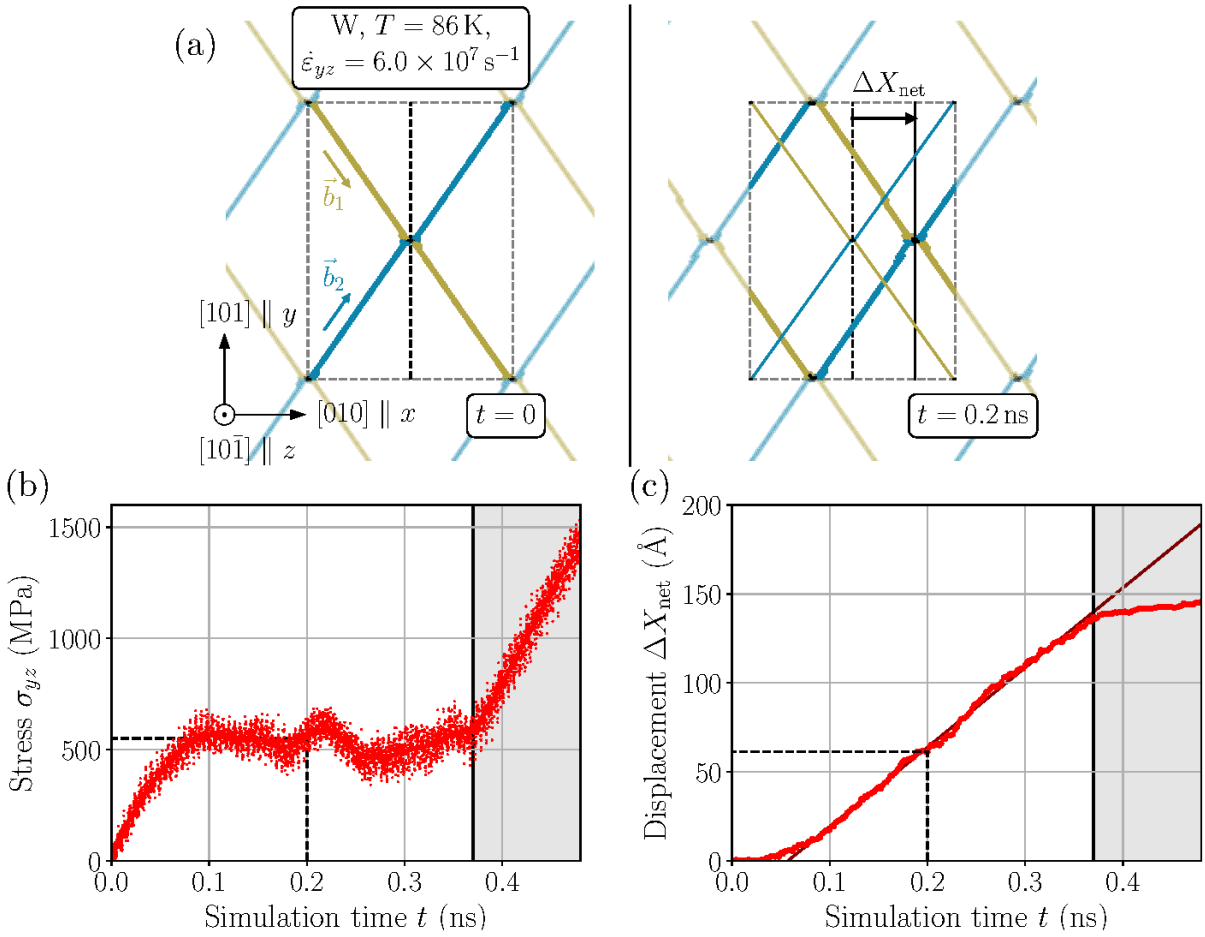

Supplementary Figure 5: Glide of a coplanar dislocation network in tungsten.
The two snapshots for $t = 0$ and 0.2 ns of the MD simulation with $\dot{\varepsilon}_{yz} = 6 \times 10^7$ s^{-1} and $T = 86$ K in the upper panel (a) shows the displacement of the network in its $(10\bar{1})$ glide plane. The time evolution of the stress component σ_{yz} existing in the simulation cell and of the displacement ΔX_{net} of the network in the X direction are respectively shown in (b) and (c). The initial configuration in $t = 0$ has been relaxed at 0 K before MD simulation.

Two intersecting $1/2\langle 111\rangle$ screw dislocations do not form spontaneously a $[010]$ junction in tungsten, as observed in previous molecular statics simulations (Fig. 4b) or predicted by the line energy model. Atomic relaxation by molecular statics leads to the same result for a planar dislocation network formed by a periodic array of intersecting $1/2\langle 111\rangle$ dislocations aligned along their screw orientation (Supplementary Fig. 5a).

At finite temperature ($T = 86$ K) and under an imposed strain rate $\dot{\varepsilon}_{yz} = 6 \times 10^7$ s^{-1}, the network starts to glide (Supplementary Fig. 5) for a corresponding stress component σ_{yz} fluctuating around 500 MPa. The motion of the network operates through nucleation of kinks at the node in the direction of the applied shear strain, with the right part of the network moving first by an elementary step before the left part follows. The glide mechanism of the network is therefore similar to the dynamic formation of $[010]$ junction in tungsten discussed in the main text. But now, because of the periodicity of the network, the kinks, which nucleate on the right of the node, eliminate on its left part after having travelled all along the screw dislocation arms, thus leading to the network glide. Such a coplanar motion observed in MD simulations agrees with the cooperative glide mechanism which has been proposed in previous studies, all based on 0 K atomic simulations[17,18,19]. However, our MD simulations show that the steady motion of the network stops at a given time, indicated by a black vertical line in Supplementary Fig. 5c, with the network being immobile thereafter. After this point, the stress component σ_{yz} starts increasing again, as the imposed strain is not accommodated anymore by the motion of the dislocation network. The locking configuration reached by the network is presented in Supplementary Fig. 6.

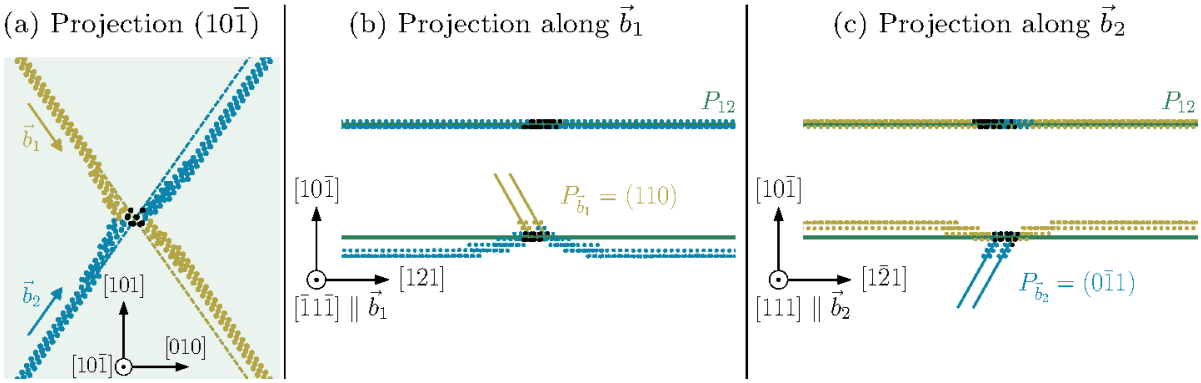

Supplementary Figure 6: Locking of a dislocation network in tungsten.
Configuration reached by the dislocation network during the MD simulation shown in Supplementary Figure 5 when the network becomes immobile, i.e. for $t \geq 0.37$ ns. The network is shown in projection in its initial $P_{12} = (10\bar{1})$ glide plane in (a), and in projection orthogonal to the two screw orientations $[\bar{1}1\bar{1}]$ and $[111]$, respectively in (b) and (c). In these two last cases, the initial and the blocking configurations are represented above and below respectively. One can see that the blocking of the network arises from dislocation cross-slip out of the P_{12} network glide plane.

In the blocking configuration (Supplementary Fig. 6), the two screw dislocations composing the network have cross-slipped in two $\{110\}$ planes different from the $P_{12} = (10\bar{1})$ glide plane of the network. The kinks created on screw dislocations by this cross-slip motion travel all along the dislocation arms but do not manage anymore to eliminate on the network node. As these kinks have a line direction with a component orthogonal to the P_{12} plane, they cannot glide in this plane, thus blocking further motion of the network. The stress starts building up, sometimes leading to additional

cross-slip events, but no further glide of the network in the P_{12} plane is observed once the blocking configuration has been reached.

b. Results in niobium

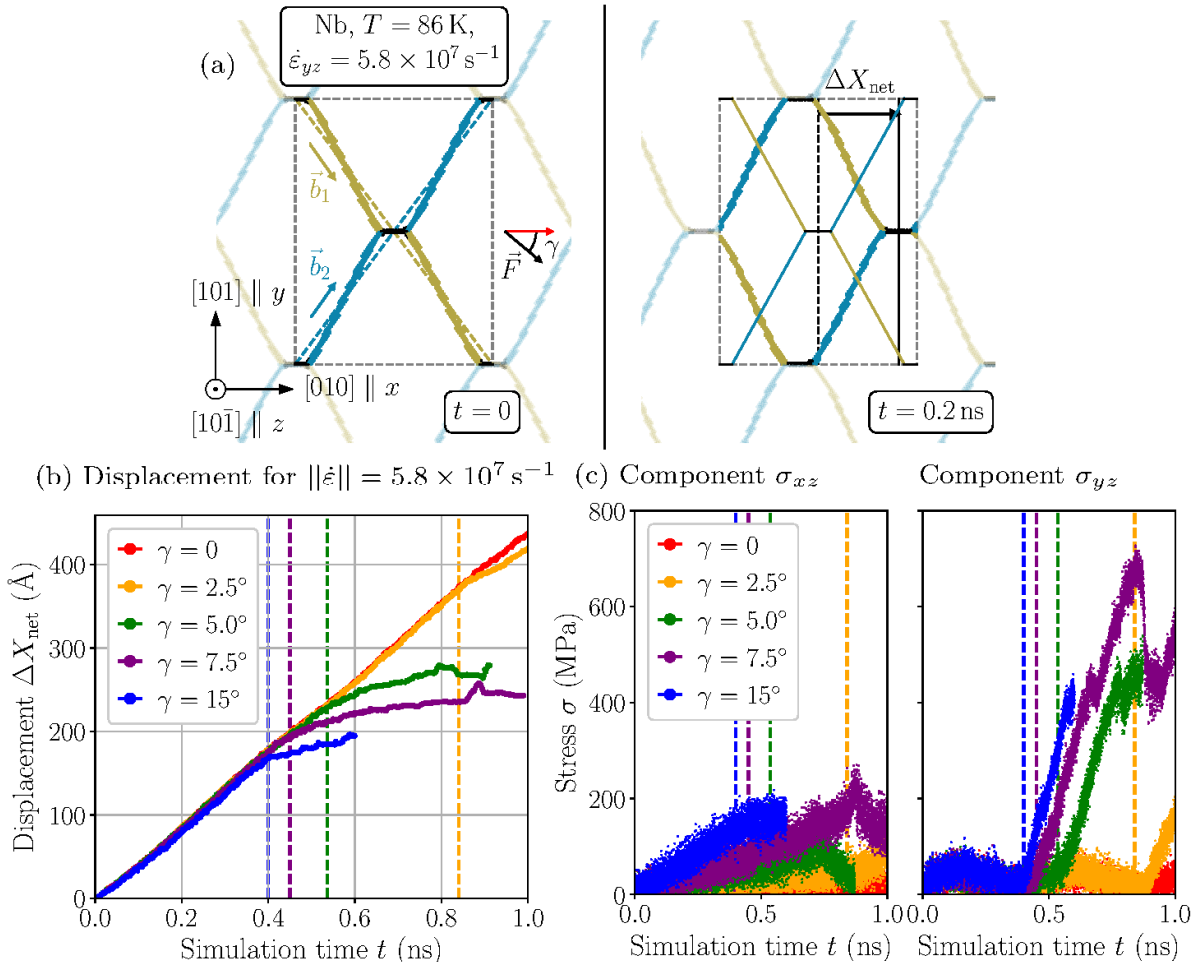

Supplementary Figure 6: Cooperative glide and locking of a dislocation network in niobium.
(a) Two snapshots of the MD straining simulation in Nb showing the initial relaxed configuration of the network and the configuration reached at $t = 0.2$ ns after glide of the network over a distance ΔX_{net}. Dashed coloured lines in the left panel indicate the screw orientations of $\vec{b}_1$ and $\vec{b}_2$ dislocations. The angle γ between orientation of the applied shear in $P_{12} = (10\bar{1})$ plane and X direction is equal to zero in this MD simulation. Time evolution of (b) the network displacement ΔX_{net} and (c) the stress components σ_{xz} and σ_{yz} for different orientations γ of the imposed shear and for a same strain rate $\dot{\varepsilon} = 5.8 \times 10^7$ s^{-1} and temperature $T = 86$ K. The vertical dashed lines indicate the time where the network starts to block.

The same simulations performed in niobium lead to a slightly different behaviour than in tungsten. Starting from the same setup, a different relaxed configuration is obtained in niobium because of the lower anisotropy ratio ($A = 0.5$ in Nb instead of 1 in W). Relaxation of the coplanar network formed by the intersection of $1/2\langle 111\rangle$ screw dislocations leads to the formation of $[010]$ junctions with a non-negligible length (left panel of Supplementary Fig. 6a), while $1/2\langle 111\rangle$ dislocations lose their

screw character and become mixed. Given the mixed character of the $1/2\,\langle 111\rangle$ dislocations, the network starts moving in MD simulations as soon as the strain is applied, with a negligible shear stress measured in the simulations cell (Supplementary Fig. 6b and d for $\gamma = 0$). The network glides over a long distance in its $P_{12} = (10\bar{1})$ habit plane, without any blocking event observed during the MD simulation. However, this is true when the applied strain corresponds to a shearing of the P_{12} plane exactly in the X direction. For this orientation, the applied shear strain leads to the same Peach-Koehler force on the two $1/2\,\langle 111\rangle$ dislocations composing the network. When the shearing of the P_{12} plane differs from X direction ($\gamma \neq 0$), the network glides as a whole over a given distance, but locks further during the simulation, even when the deviation angle γ is as small as 2.5° (Supplementary Fig. 6). This is a consequence of the small asymmetry of the applied strain, resulting in different driving forces on each dislocation. Because of this imbalance, one dislocation arm moves faster than the other one and finally aligns along its screw orientation. This allows for cross-slip on the dislocation in a different plane than the network glide plane, leading to a locking configuration similar to the one observed in tungsten (Supplementary Fig. 5).

c. Discussion

A locking of dislocation networks is thus observed in both tungsten and niobium. This locking operates when the $1/2\,\langle 111\rangle$ dislocations align along their screw orientation, thus allowing for their cross-slip out of the network glide plane. In tungsten, as $1/2\,\langle 111\rangle$ dislocations are already along their screw orientation in the relaxed network, cross-slip and network locking operates readily. In niobium, a simple perturbation of the mechanical loading, corresponding to a deviation from a pure shear of the $(10\bar{1})$ along the $[010]$ direction, leads to this critical configuration. These MD simulations agree with our TEM in situ tensile experiments in niobium showing that such networks difficulty glide. They also confirm that imperfect networks could not rapidly glide as a whole over long distances, as sometimes proposed to explain anomalous slip in BCC metals.

References

62. Hirth, J.P. & Lothe, J. *Theory of dislocations* (Wiley, New York, 1982).
63. Bolef, D.I. Elastic constants of single crystals of the BCC transition elements V, Nb, and Ta. *J. Appl. Phys.* **32**, 100–105 (1961).
64. Keith, J.C. Elastic constants of niobium from 4.2 to 300 K. *J. Appl. Phys.* **36**, 3689–3690 (1965).
65. Bolef, D.I. & de Klerk, J. Anomalies in the elastic constants and thermal expansion of chromium single crystals. *Phys. Rev.* **129**, 1063–1067 (1963).
66. Bolef, D.I. & de Klerk, J. Elastic constants of single-crystal Mo and W between 77 and 500 K. *J. Appl. Phys.* **33**, 2311–2314 (1962).
67. Dever, D.J. Temperature dependence of the elastic constants in α-iron single crystals: relationship to spin order and diffusion anomalies. *J. Appl. Phys.* **43**, 3293–3301 (1972).
68. Bulatov, V.V. & Cai, W. *Computer simulations of dislocations* (Oxford Univ. Press, Oxford, 2006).
69. DDLab; http://micro.stanford.edu/~caiwei/Forum/2005-12-05-DDLab/
70. Bertin, N., Cai, W., Aubry, S. Bulatov, V.V. Core energies of dislocations in BCC metals. *Phys. Rev. Mater.* **5**, 025002 (2021).
71. Foreman, A.J.E. Dislocation energies in anisotropic crystals. *Acta Metall.* **3**, 322–330 (1955).
72. Head, A.K. The energy of a screw dislocation in a cubic crystal. *Phys. Stat. Sol. (b)* **5**, 51–54 (1964).
73. Head, A.K. The [111] dislocation in a cubic crystal. *Phys. Stat. Sol. (b)* **6**, 461–465 (1964).